Interfacial Flow around Brownian Colloids

Article *in* Physical Review Letters · June 2021

DOI: 10.1103/PhysRevLett.126.228003

5 authors, including:

Mehdi Molaei
University of Pennsylvania
16 PUBLICATIONS **330** CITATIONS

Featured in Physics

Interfacial Flow around Brownian Colloids

Mehdi Molaei, Nicholas G. Chisholm, Jiayi Deng, John C. Crocker, and Kathleen J. Stebe*
Chemical and Biomolecular Engineering, University of Pennsylvania, Philadelphia, Pennsylvania 19104, USA

(Received 14 July 2020; revised 21 March 2021; accepted 8 April 2021; published 2 June 2021)

Understanding the flow created by particle motion at interfaces is a critical step toward understanding hydrodynamic interactions and colloidal self organization. We have developed correlated displacement velocimetry to measure flow fields around interfacially trapped Brownian particles. These flow fields can be decomposed into interfacial hydrodynamic multipoles, including force monopole and dipole flows. These structures provide key insights essential to understanding the interface's mechanical response. Importantly, the flow structure shows that the interface is incompressible for scant surfactant near the ideal gaseous state and contains information about interfacial properties and hydrodynamic coupling with the bulk fluid. The same dataset can be used to predict the response of the interface to applied, complex forces, enabling virtual experiments that produce higher order interfacial multipoles.

DOI: 10.1103/PhysRevLett.126.228003

Brownian motion of particles at interfaces reveals the complex physics of these layers via the fluctuation dissipation theorem (FDT). The FDT guarantees that the measurement based on Brownian motion, as here, and an active measurement must have strictly corresponding mechanical properties. Thermal energy moves a particle, and the resulting flow generates a resisting drag force [1–3]. These thermally induced flows result in correlated motion of the particles, used in techniques like two-point microrheology [4–10] to measure the rheological properties of fluids and to understand many biological processes [11–14]. Here, we introduce "correlated displacement velocimetry" (CDV) to measure and visualize the field of nanoscale displacement induced by one or more colloidal particles undergoing thermal motion.

The far field displacement due to motion of a single colloid approximates the interfacial flow field induced by a point force on the interface, which we term an interfacial Stokeslet. Simultaneous motion of multiple particles generates higher order flow singularities. We measure these higher order flow singularities by designing *virtual* experiments that map out displacement fields induced by the relative motion of particles. Through these virtual experiments, we can predict the outcome of applying forces to multiple points by averaging over a subensemble of the data.

The measured displacement field provides key insights for flow structures essential to understand mechanical response of the interface. Through this measurement, for instance, we show that a fluid interface with trace surface active compound is incompressible, while the surface pressure is detectable only using the most stringent methods, e.g., micromanometry [15,16]. Furthermore, particular aspects of the flow structure depend on the surface viscosity and the contribution of bulk forces. This dependence provides a window to bound the surface viscosity with exquisite sensitivity. Thus, we are able to detect the presence of scant surfactant by visualization of the flow structure and by bounding the surface viscosity to be less than 1×10^{-10} Pa s m. The far field flow induced by higher order force singularities confirms the linear response of this interfacial system.

Throughout this Letter, we study the motion of particles at the interface of a viscous fluid. The displacement field $\boldsymbol{U}$ measured over small lag time τ is related to the velocity field by $\boldsymbol{u} \approx \boldsymbol{U}(\tau)/\tau$. By determining $\boldsymbol{U}$, we measure the flow around micron size colloids undergoing purely Brownian motion. Spheres with diameter $a = 1$ μm, trapped at the air-water interface, Fig. 1(a), diffuse over time. We track the particles over time t by careful particle tracking [17,18]. We then calculate their displacement as a function of lag time τ as $\Delta\boldsymbol{r}^i(t,\tau) = \boldsymbol{r}^i(t+\tau) - \boldsymbol{r}^i(t)$, where $\boldsymbol{r}^i$ is the position vector of particle i. The sample vector field of displacements of individual particles, shown in Fig. 1(b), indicates no apparent spatially correlated flow field. However, by proper ensemble averaging and consideration of the correlation field, we measure the displacement field induced by the motion of these Brownian particles, Fig. 1(c).

To measure the flow field, we choose any one of these particles as a source for the displacement. We label its displacement vector $\Delta\boldsymbol{r}^s(t,\tau)$. We construct a new coordinate system with its origin centered on the source particle, $\boldsymbol{r}^s(t)$, and with the Y axis along the direction of $\Delta\boldsymbol{r}^s$, the inset of Fig. 1(b). We then transform the displacement of all other "probe" particles (labeled with superscript p) to the shifted coordinate system as $\boldsymbol{R}^{sp}(t) = \boldsymbol{r}^p(t) - \boldsymbol{r}^s(t)$. We repeat this process, allowing each particle to be a source, one at a time. Next, we form ensembles of probe particles based on their relative locations with respect to the source

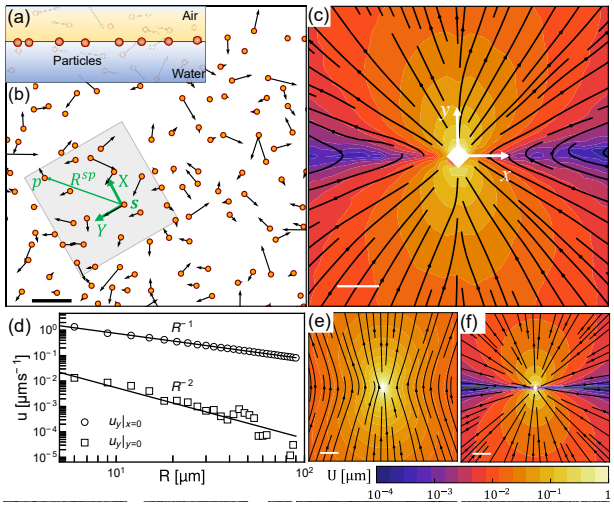

FIG. 1. (a) Particles at the air-water interface are moving randomly as shown in (b) for $\tau = 0.04$ s. Vectors are scaled up by a factor of 10^3; inset shows a coordinate system located on the original position of particle s with the Y axis aligned with particle displacement. (c) Displacement at the interface induced by the motion of colloids captured by the correlated displacement velocimetry. Streamlines indicate the local direction of the displacement, and the color scheme indicates its magnitude. The scale bar is 20 μm. (d) Spatial decay of interfacial Stokeslet; symbols show measured velocity by CDV, and lines are the best fit to $u_y|_{x=0} = \Phi_{\parallel} f$ and $u_y|_{y=0} = \Phi_{\perp} f$. Displacement field for an interfacial Stokeslet flow at (e) an ideal compressible interface and (f) an incompressible interface.

particles. The displacement field at $\boldsymbol{R}$ is then measured by conditional averaging as

$$\boldsymbol{U}(\boldsymbol{R},\tau) = \frac{\sum_s \sum_p w(\boldsymbol{R}^{sp},\boldsymbol{R})\Delta\boldsymbol{r}^p(\tau)}{\sum_s \sum_p w(\boldsymbol{R}^{sp},\boldsymbol{R})}. \tag{1}$$

Here, w is the binary weighting function given by

$$w(\boldsymbol{R}^{sp},\boldsymbol{R}) = \begin{cases} 1 & |R - R^{sp}| < \Delta R \wedge |\theta - \theta^{sp}| < \Delta\theta \\ 0 & \text{otherwise,} \end{cases} \tag{2}$$

where $R = |\boldsymbol{R}|$, $\theta^{sp} = \angle(\Delta\boldsymbol{r}^s, \boldsymbol{R}^{sp})$ gives the angle from $\Delta\boldsymbol{r}^s$ to $\boldsymbol{R}^{sp}$, and ΔR and $\Delta\theta$ are the radial and angular bin sizes, respectively. By capturing a large dataset, we ensure that the ensemble average of each bin is statistically significant, $\boldsymbol{U} > \sigma/\sqrt{N}$, where σ is the standard deviation of the displacement of all the probe particles in the ensemble, and N is the ensemble size. The displacement field shown in Fig. 1(c) is generated by the net thermal displacement of particles, 0.25 μm, over 0.04 s, and it is identical to the flow field theoretically predicted for a driven colloid trapped at an incompressible interface [19]. To capture this field, $\sim 10^{11}$ particle displacement pairs have been used [20]. To avoid high probe density, we record over prolonged times (3 min). By keeping the surface density of the probe particles small, $\psi \approx 0.001$, we also avoid formation of a 2D colloidal crystal structure [24], so electrostatic repulsion between particles can be neglected [25–27]. Supporting analysis of electrostatic repulsive forces between particles is given in Figs. S8–S9 of the Supplemental Material [20].

This procedure is in fact identical to measuring the correlation field between particles,

$$\boldsymbol{C}(\boldsymbol{R},\tau) = \langle \boldsymbol{\chi}^{sp}(t,\tau)\delta^{2D}[\boldsymbol{R} - \boldsymbol{R}^{sp}(t)]\rangle_{t,sp}, \tag{3}$$

where $\chi^{sp}_{ij}(t,\tau) = \Delta r^s_i(t,\tau)\Delta r^p_j(t,\tau)$, $\langle\cdot\rangle_{t,sp}$ is the average over time and particle pairs, and δ^{2D} is the 2D Dirac delta. $\boldsymbol{U}(\boldsymbol{R},\tau) = \langle\Delta r^2(\tau)\rangle^{-1/2}\boldsymbol{C}(\boldsymbol{R},\tau)\cdot\hat{\boldsymbol{e}}_y$ leads to the displacement field similar to Eq. (1).

The interfacial Stokeslet flow at an ideal interface, absent surface active agents, shown in Fig. 1(e), is the same as a Stokeslet in a fluid of viscosity $\eta/2$, $u_i = f_j(R_iR_j/R^3 + \delta_{ij}/R)/4\pi\eta$, where $\boldsymbol{f}$ and η are the interfacial Stokeslet strength and the sum of viscosities of two fluids above and below the interface, respectively [19]. This flow field corresponds to a compressible interface with $\boldsymbol{\nabla}_s \cdot \boldsymbol{u} = \boldsymbol{f}\cdot\boldsymbol{R}/(2\pi\eta R^3)$, where $\boldsymbol{\nabla}_s$ is the 2D (surface) gradient operator. Interestingly, however, the flow field measured in Fig. 1(c) is surface-divergence free, indicating incompressibility of the interface (Fig. S1 of the Supplemental Material [20]). Therefore, the measured flow field, remarkably, shows the pronounced effect of trace surfactant rendering the interface incompressible. This observation indicates that, for the thermally induced flow field, viscous stresses are so weak that Marangoni stresses significantly reorganize the interfacial flows even for a highly expanded surfactant film in a surface gaseous state [19].

While in our experiments, we took pains to avoid surfactant contamination, the surface pressures $\Pi < 8 \times 10^{-5}$ N m^{-1} (see Fig. S3 of the Supplemental Material [20]), likely from trace impurities related to water sample, the experiment cylindrical vessel, and the probe particles [28]. To remove ambiguity of the effect of impurities on the flow field, we form a monolayer of 1-decanol surfactant at the air-water interface in the gaseous state (see Sec. IX of the Supplemental Material [20]). For this deliberately added surfactant in the gaseous state, the surface pressure gradient is strong enough to render the interface incompressible. The relative importance of surface pressure gradients to viscous stresses is captured in the Marangoni number Ma. The importance of the surface diffusivity of surfactant molecules can be captured by the product of the Marangoni and Peclet numbers for the thermally driven system, $Ma = \bar{\Gamma}\sqrt{k_BTa\tau/\eta}$, where $\bar{\Gamma}$ is the average surface concentration of surface active agents, k_B is Boltzmann's constant, and T is the temperature. Furthermore, we show that $MaPe = \bar{\Gamma}a_s a$, where $a_s = k_BT/D_s\eta$ is the effective size of the surfactant molecules, and D_s is its diffusion coefficient [20]. Further, analysis

suggests that efforts to remove surfactant from the interface would not remove this effect. To extract a bounding value for Ma in the most stringent circumstance, we consider undetectable surface pressure $\Pi = 10^{-5}$ N m^{-1}, where the surfactant concentration is as small as $\bar{\Gamma} = 10^3$ molecules/μm^2. For this concentration, we estimate $Ma \approx 400$ and $MaPe \approx 40$, indicating that Brownian motion of particles cannot compress the interface even for highly expanded gaseous monolayers of surfactant, and surface diffusivity of surfactant is insufficient to generate mass flux. We expect that this incompressible interfacial Stokeslet flow field is typical for interfacially trapped colloids moving under external forces, in systems with high Ma and scant surfactant [19,29].

Subtle features in this measured flow field are important in understanding the interfacial mechanics. A point force exerted at distance $|z| = h$ from an interface that is both incompressible and has finite surface viscosity η_s induces an interfacial flow field

$$u_i = \frac{\Phi_0 - \Phi_2}{4\pi\eta} f_i + \frac{\Phi_2}{2\pi\eta R^2} R_i R_j f_j, \tag{4}$$

where $\Phi_n(l_s; R, z) = \int_0^\infty dk e^{-kh} J_n(kR)/(1 + l_s k)$, J_n is the Bessel function of the first kind of order n, and $l_s = \eta_s/\eta$ [19]. This response of the interface to the point force depends explicitly on the ratio of the surface to bulk viscosity and implicitly on the Marangoni stresses that enforce the incompressibility of the interface. The corresponding asymptotic form for the $l_s \ll R$ and $h \ll R$

$$u_i = (\Phi_\parallel - \Phi_\perp) \frac{R_i R_j f_j}{R^2} + \Phi_\perp f_i + O(R^{-3}), \tag{5}$$

where $\Phi_\parallel = (2\pi\eta R)^{-1}$ and $\Phi_\perp = (l_s + h)(2\pi\eta R^2)^{-1}$, shown in Fig. 1(f). The system, for force in the y direction, has y-directed flow on the axes of $u_y|_{x=0} = \Phi_\parallel f$ and $u_y|_{y=0} = \Phi_\perp f$ (see Supplemental Material [20]).

Figure 1(d) shows the velocity along the y and x axes obtained from the displacement map in Fig. 1(c). We estimate the interfacial Stokeslet strength to be $f = 4.7 \times 10^{-14}$N by fitting $\Phi_\parallel f$ to the measured values $u_y|_{x=0}$ and assuming $\eta = 1.0$ mPa s. The observed uniform $1/R$ decay of $u_y|_{x=0}$ indicates that the measurement domain corresponds to a far-field regime for which $R \gg l_s$; otherwise, the flow would have decayed logarithmically. Further, the observed $u_y|_{y=0}$ decays as $1/R^2$, also in agreement with far-field prediction; the predicted dependence of this quantity on l_s and h allows bounding values to be extracted. Fitting $u_y|_{y=0}$ in Fig. 1(d) to its predicted form with $h = 0$, we find the upper bound on $l_s = 0.073$ μm, providing an upper bound on the surface viscosity of $\eta_s = 7.3 \times 10^{-11}$ Pa s m. A particle trapped at the interface, however, exerts forces on the interface and the bulk fluids by point forces distributed over the entire probe surface. When $l_s < a$, contributions of the bulk force on the interfacial flow cannot be neglected *a priori*. In this case, $\Phi_\perp \simeq (l_s + l_b)(2\pi\eta R^2)^{-1}$, where l_b is a length scale that establishes the net effect of the bulk force on the interfacial flow. Interestingly, our flow measurement indicates that l_b cannot be larger than 0.073 μm for our 1 μm probes. This upper bound on l_b indicates that the drag force on the particle is mainly located near the interface. A similar result is observed in the monolayer of 1-decanol surfactant in the gaseous state; see Fig. S12 of the Supplemental Material [20].

It is possible for the probe particles themselves to form a 2D viscous suspension at the fluid interface. However, in all data reported here, the surface concentration is sufficiently dilute (approximately 100 spherical particles in the field of view with area of $A = 0.2$ mm^2) that such effects are negligible. For $\psi \ll 0.1$, the surface viscosity induced by the particles can be estimated as $\eta_s^{\text{particles}} \approx 0.9\eta a\psi$ [30] which means in our system $\eta_s^{\text{particles}} \approx 0.9 \times 10^{-13}$ Pa s m. Thus, while the 2D suspension of particles could, in principle, contribute to the surface viscosity, this effect is negligible in our system.

By the FDT, the rms magnitude of the net stochastic force acting on particles in a purely viscous system [31] over $\tau \gg m/\gamma$ is $f_{\text{rms}} = \sqrt{2\gamma k_B T/\tau}$, where γ and m are the drag coefficient and mass of the particle. This allows us to extract a value for the drag coefficient on our particles from our measurement. (FDT holds for our system since the interface is linear, incompressible, and in equilibrium; see Fig. S7 of the Supplemental Material [20]. These properties preclude anomalous collective diffusion of colloidal particles predicted for particles on a compressible fluid-fluid interface [32–34]).

Using the force value fit to the far field flow velocity, we estimate $\gamma = 1.09 \times 10^{-8}$ Pa s m. We confirm the reliability of the CDV method by comparing this estimate to the drag coefficient determined by conventional particle tracking. By investigating the thermal motion of individual particles through analyzing their mean squared displacement (Fig. S5 of Ref. [20]), we determine their translation diffusion coefficient D. We obtain the drag coefficient of each particle using the Stokes-Einstein equation, $\gamma = k_B T/D$, and find a wide distribution of drag coefficients, Fig. 2(a). This broad distribution is consistent with the literature, and associated with different trapped wetting states [35]. The median value of the drag coefficients, $\gamma = 1.06 \pm 0.16 \times 10^{-8}$ Pa s m, agrees well with the value estimated from the far field flow, benchmarking the CDV method. The broad distribution of γ from analysis of the individual particles cannot be attributed to interface inhomogeneities, as there is no clear correlation between particle mobility and their location at the interface Fig. 2(b), and the characteristic decay rate of the displacement field indicates that the interface is a course-grained homogeneous system [10,36].

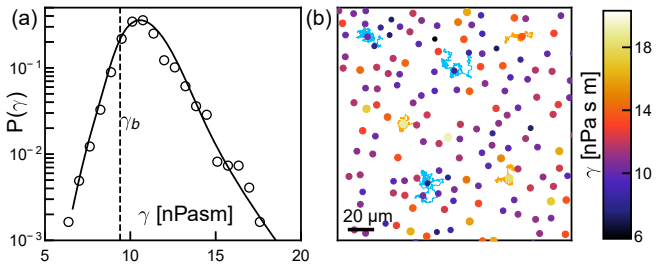

FIG. 2. (a) Distribution of the drag coefficient; symbols are measured value with line showing the best fit to the model. (b) Drag coefficient of particles at different neighborhood of the interface. Color and size of each circle indicate its drag coefficient. The sample trajectories with large and small mobility are shown with blue and orange lines, respectively.

This finding indicates that ensemble motion of particles is insensitive to variation in wetting behavior of individual probes. Finally, we note that although interfacially trapped particles are only partially immersed in water, their average drag coefficient is 15% larger than the drag coefficient for the 3D motion of a probe particle in the bulk fluid, $\gamma_b = 3\pi\eta a = 9.4 \times 10^{-9}$ Pa s m, a known and interesting effect subject to ongoing discussion.

From a purely hydrodynamic perspective, the drag on the spherical particles with contact angle ϕ moving in an incompressible interface with small Boussinesq number $Bo = l_s/a \ll 1$ obeys the relationship $\gamma/\gamma_b = (8/3\pi)\cos(\phi/2)$ [2,37], which does not predict larger drag on particles at the interface over those in the bulk. We also estimate that the maximum contribution of surface viscosity in the total drag on the particle is under 6% [20] based on the bounding value for surface viscosity, as determined from the far field flow. Boniello *et al.* have reported such an increase in the drag for particles at the interface and have shown that as particles protrude more into the less viscous air phase they diffuse more slowly [38,39]. They propose mechanisms associated with hydrodynamic or thermal consequences of contact line (de) pinning to explain this increased dissipation. However, the source of such an increase in the drag coefficient remains a subject of debate [38–42] and is beyond the scope of the current study. Nevertheless, the wide range of the distribution of drag coefficients observed here suggests that particles are trapped at different heights at the interface [38,43,44] and feel different drag. To characterize the observed distribution, we consider γ as a function of contact angle as reported in Ref. [38], $\gamma = \gamma_b F(\phi)$, where γ_b and ϕ are random variables with normal distribution, and F is an empirical relation that follows the experimental data; see Fig. S6 of the Supplemental Material [20]. Since γ_b and ϕ are independent random variables, we can determine the probability distribution of drag coefficient through $P(\gamma) = \int_{-\infty}^{\infty} P_{\gamma_b}(\gamma_b) P_F(\gamma/\gamma_b)/\gamma_b d\gamma_b$, where $P_F(F) = P_\phi(\phi)/(dF/d\phi)$ [20]. A narrow range of particle contact angle, $\phi = 114.0 \pm 10.5°$, which agrees with the reported behavior for polystyrene latex particles spread at an air-water interface [35], and particle size $a = 1.00 \pm 0.08$ μm predict the distribution of the drag coefficient as shown in Fig. 2(a).

So far, we have measured the interfacial Stokeslet flow by analyzing displacement induced by the thermal motion of individual particles. Here, we use the relative motion of particles to measure the flow fields induced by higher order singularities such as interfacial stresslets. We call these measurements virtual experiments in that we measure the far field flow of higher order singularities while there are no real forces in the center of the flow fields. Let us consider two particles, $s1$ and $s2$, at distance l_d from each other; the far field flow induced by relative motion of this pair of particles will be equivalent to flow around an interfacial force dipole that acts at their mutual center of mass, $\boldsymbol{r}^s(t) = [\boldsymbol{r}^{s1}(t) + \boldsymbol{r}^{s2}(t)]/2$. To measure this flow field, we need only to set up a new ensemble of source displacements from pairs of particles that are located at distance l_d from each other with unit vector of the line between them as $\hat{\boldsymbol{e}}^s(t) = [\boldsymbol{r}^{s1}(t) - \boldsymbol{r}^{s2}(t)]/[|\boldsymbol{r}^{s1}(t) - \boldsymbol{r}^{s2}(t)|]$. The relative motion along $\hat{\boldsymbol{e}}^s$ (extensional mode) is

$$\Delta r^s_{\parallel}(t,\tau) = [\Delta \boldsymbol{r}^{s1}(t,\tau) - \Delta \boldsymbol{r}^{s2}(t,\tau)]\cdot\hat{\boldsymbol{e}}^s(t), \tag{6}$$

and their relative motion normal to $\hat{\boldsymbol{e}}^s$ (shear mode) is

$$\Delta r^s_{\perp}(t,\tau) = [\Delta \boldsymbol{r}^{s1}(t,\tau) - \Delta \boldsymbol{r}^{s1}(t,\tau)]\cdot(\hat{\boldsymbol{e}}^s(t) \times \hat{\boldsymbol{e}}_z). \tag{7}$$

To measure $\boldsymbol{U}$ induced by these dipolar modes, we locate the coordinate system at $\boldsymbol{r}^s(t)$ and align the Y axis with $\hat{\boldsymbol{e}}^s(t)$ to form $\boldsymbol{R}^{sp}$ that connects the center of the dipole to the position of probe particles. We then measure the correlation of the probes' displacements with the relative motion of particle pairs, $\boldsymbol{C} = \Delta r^s_{\parallel,\perp}(t,\tau)\Delta \boldsymbol{r}^p(t,\tau)$ and finally perform following conditional averaging,

$$\boldsymbol{U}(\boldsymbol{R}) = \frac{\sum_s \sum_p w(\boldsymbol{R}^{sp},\boldsymbol{R})\boldsymbol{C}}{\langle|\Delta r^s_{\parallel,\perp}|\rangle \sum_s \sum_p w(\boldsymbol{R}^{sp},\boldsymbol{R})}. \tag{8}$$

The predicted response of the interface to a force dipole for $l_s \ll a$ is obtained by taking the gradient of Eq. (5) with respect to $\boldsymbol{R}$, which gives the dipole moment

$$u_i = \frac{q_{jk}}{2\pi\eta}\left[\left(3 - 4\frac{l_s + l_b}{R}\right)\frac{R_i R_j R_k}{R^5} - \left(1 - \frac{l_s + l_b}{R}\right)\frac{R_i\delta_{jk} + R_j\delta_{ik}}{R^3} + 2\frac{(l_s + l_b)\delta_{ij}R_k}{R^4}\right] \tag{9}$$

to $O(R^{-4})$, where q_{jk} is the dipole strength. Figures 3(a) and 3(c) reveal the flow induced by a dipole formed by the

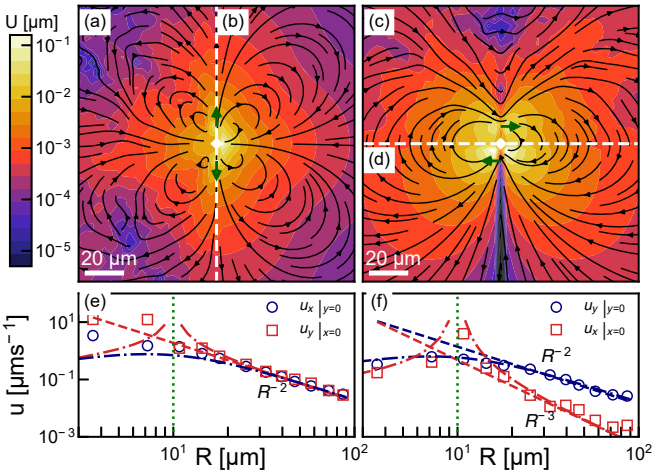

FIG. 3. (a) and (c) Displacement, $\boldsymbol{U}$, generated by virtual force dipoles exerted at interface by relative motion of particles pairs moving parallel (a) and normal (c) to their interparticle distance for $\tau = 0.04$ s. (b) and (d) Analytical force dipole flows obtained from the best fit to Eq. (9). Streamlines indicate the local direction of the displacement, and the color contours indicate velocity magnitude. (e)–(f) Spatial decay of the flow field, $\boldsymbol{u}$, along x and y axis. Symbols are the measured velocity, dashed lines are the best fit to force dipole flows, and dot-dashed lines are the best fit to the flow due to a pair of Stokeslets centered at $y = \pm 10$ μm.

motion of particles pairs, $\Delta r_{\parallel}^{s}$ and $\Delta r_{\perp}^{s}$, respectively, with $l_d = 20 \pm 2$ μm and moving over $\tau = 0.04$ s.

The measured displacement fields accurately capture all the far-field components of the theoretical force dipoles displayed at Figs. 3(b) and 3(d) for q_{22} and q_{12}, respectively. For the extensional force dipole, or "interfacial stresslet" [Figs. 3(a)–3(b)], the displacement field displays characteristic $1/R^2$ decay, Fig. 3(e). However, the flow induced by the sheared force dipole decays with two different characteristic rates. Parallel to the shear direction, the momentum is mainly transferred by the bulk viscosity and the surface incompressibility, and flow decays with $1/R^2$, while normal to the shear direction, the flow decays with $1/R^3$ due to the surface viscosity and bulk forces, Fig. 3(f).

In the near field, there is some deviation between the measured flow and that theoretically predicted by the interfacial force dipole (9), mainly because of finite physical distance between two source particles in the measurement. By mathematically superimposing a pair of shifted interfacial Stokeslets (5), one for each particle, we predict the near-field measurement with improved accuracy, Figs. 3(e)–3(f). This superimposability of the interfacial flow is expected for a linear viscous and incompressible system. However, for $R \gg l_d$, the far-field approximation provided by the extensional and shear interfacial dipoles is accurate, Figs. 3(e)–3(f). From the best fit to the measured flow, we obtained $|q_{22}| = 9.8 \times 10^{-19}$ N m, which agrees well with $fl_d = 9.4 \times 10^{-19}$ N m. Furthermore, for particle pairs, by separating those that move toward and away from each other into distinct ensembles (i.e., based on the sign of $\Delta r_{\parallel}$), we measure both extensile $q_{22} > 0$ and contractile $q_{22} < 0$ interfacial stresslets; see Fig. S13 of the Supplemental Material [20]. The far field flow induced by these force dipoles are simply opposite in sign, another hallmark of this system's linear response to forces. Similarly, we find a shear dipole strength of $|q_{12}| = 9.6 \times 10^{-19}$ N m. An interfacial rotlet can be reconstructed from shear dipoles with a torque equal to $L = (q_{12} - q_{21})/2$.

In this study, we demonstrate that correlated displacements of collections of particles reveal the mechanics of a weakly viscous, incompressible, Newtonian interface. We confirmed the reliability of the CDV method by the agreement of drag coefficients inferred from the far-field flow and from the mobility of the particles. The agreement of the analytical and experimental forms of flow fields for force monopoles and dipoles further support confidence in our method. The CDV method could be adapted to address non-Newtonian interfaces with potentially nonlinear mechanics; studies of the relative motion of particle collections to reveal purely shear or purely extensional displacement fields could independently measure shear [45,46] and extensional [47–49] surface viscosities. CDV could also help to understand the hydrodynamic coupling between interfaces and bulk fluids [50]. Flow induced by higher order singularities provides insight for flows induced by active colloids and active rheological probes. For instance, a bacterium swimming at an interface is predicted to generate a flow similar to a force dipole [19]. The flow measured around interfacially trapped bacteria is the subject of our ongoing research.

We thank the reviewers whose comments immensely improved this letter. We acknowledge partial support for N. G. C., M. M., and J. D. from NSF-DMR 1607878 and partial support for M. M. from Grant No. 55120-NDS from the ACS Petroleum Research Fund.

*Corresponding author.
kstebe@seas.upenn.edu

[1] A. J. Levine and F. C. MacKintosh, Phys. Rev. E **66**, 061606 (2002).
[2] T. M. Fischer, P. Dhar, and P. Heinig, J. Fluid Mech. **558**, 451 (2006).
[3] G. J. Elfring, L. G. Leal, and T. M. Squires, J. Fluid Mech. **792**, 712 (2016).
[4] V. Prasad, S. A. Koehler, and E. R. Weeks, Phys. Rev. Lett. **97**, 176001 (2006).
[5] V. Prasad and E. R. Weeks, Phys. Rev. Lett. **102**, 178302 (2009).
[6] M. H. Lee, D. H. Reich, K. J. Stebe, and R. L. Leheny, Langmuir **26**, 2650 (2010).

[7] M. Molaei and J. C. Crocker, J. Colloid Interface Sci. **560**, 407 (2020).
[8] T. T. Hormel, M. A. Reyer, and R. Parthasarathy, Biophys. J. **109**, 732 (2015).
[9] M. Sickert, F. Rondelez, and H. A. Stone, Europhys. Lett. **79**, 66005 (2007).
[10] J. C. Crocker, M. T. Valentine, E. R. Weeks, T. Gisler, P. D. Kaplan, A. G. Yodh, and D. A. Weitz, Phys. Rev. Lett. **85**, 888 (2000).
[11] S. Ramadurai, A. Holt, V. Krasnikov, G. van den Bogaart, J. A. Killian, and B. Poolman, J. Am. Chem. Soc. **131**, 12650 (2009).
[12] A. Naji, A. J. Levine, and P. A. Pincus, Biophys. J. **93**, L49 (2007).
[13] F. Höfling and T. Franosch, Rep. Prog. Phys. **76**, 046602 (2013).
[14] G. Vereb, J. Szöllősi, J. Matkó, P. Nagy, T. Farkas, L. Vígh, L. Mátyus, T. A. Waldmann, and S. Damjanovich, Proc. Natl. Acad. Sci. U.S.A. **100**, 8053 (2003).
[15] N. R. Pallas and B. A. Pethica, J. Chem. Soc., Faraday Trans. **83**, 585 (1987).
[16] N. R. Pallas and B. A. Pethica, Phys. Chem. Chem. Phys. **11**, 5028 (2009).
[17] J. C. Crocker and D. G. Grier, J. Colloid Interface Sci. **179**, 298 (1996).
[18] K. A. Rose, M. Molaei, M. J. Boyle, D. Lee, J. C. Crocker, and R. J. Composto, J. Appl. Phys. **127**, 191101 (2020).
[19] N. G. Chisholm and K. J. Stebe, J. Fluid Mech. **914**, A29 (2021).
[20] See Supplemental Material at http://link.aps.org/supplemental/10.1103/PhysRevLett.126.228003 for additional information about the experimental setup, divergence field measurement, and derivation of drag coefficient and Marangoni number, which includes Refs. [21–23].
[21] S. Y. Lin, K. McKeigue, and C. Maldarelli, Langmuir **7**, 1055 (1991).
[22] D. O. Johnson and K. J. Stebe, J. Colloid Interface Sci. **182**, 526 (1996).
[23] N. B. Vargaftik, B. N. Volkov, and L. D. Voljak, J. Phys. Chem. Ref. Data **12**, 817 (1983).
[24] L. Parolini, A. D. Law, A. Maestro, D. M. A. Buzza, and P. Cicuta, J. Phys. Condens. Matter **27**, 194119 (2015).
[25] B. J. Park, J. Vermant, and E. M. Furst, Soft Matter **6**, 5327 (2010).
[26] C. P. Kelleher, A. Wang, G. I. Guerrero-García, A. D. Hollingsworth, R. E. Guerra, B. J. Krishnatreya, D. G. Grier, V. N. Manoharan, and P. M. Chaikin, Phys. Rev. E **92**, 062306 (2015).
[27] R. Aveyard, B. P. Binks, J. H. Clint, P. D. I. Fletcher, T. S. Horozov, B. Neumann, V. N. Paunov, J. Annesley, S. W. Botchway, D. Nees, A. W. Parker, A. D. Ward, and A. N. Burgess, Phys. Rev. Lett. **88**, 246102 (2002).
[28] M. Rey, T. Yu, R. Guenther, K. Bley, and N. Vogel, Langmuir **35**, 95 (2019).
[29] J. Bławzdziewicz, V. Cristini, and M. Loewenberg, Phys. Fluids **11**, 251 (1999).
[30] S. V. Lishchuk and I. Halliday, Phys. Rev. E **80**, 016306 (2009).
[31] R. Kubo, Rep. Prog. Phys. **29**, 255 (1966).
[32] J. Bleibel, A. Domínguez, and M. Oettel, J. Phys. Condens. Matter **27**, 194113 (2015).
[33] J. Bleibel, A. Domínguez, and M. Oettel, J. Phys. Condens. Matter **28**, 244021 (2016).
[34] R. P. Peláez, F. B. Usabiaga, S. Panzuela, Q. Xiao, R. Delgado-Buscalioni, and A. Donev, J. Stat. Mech. (2018) 063207.
[35] V. N. Paunov, Langmuir **19**, 7970 (2003).
[36] A. J. Levine and T. C. Lubensky, Phys. Rev. Lett. **85**, 1774 (2000).
[37] T. M. Fischer, Phys. Rev. Lett. **92**, 139603 (2004).
[38] G. Boniello, C. Blanc, D. Fedorenko, M. Medfai, N. B. Mbarek, M. In, M. Gross, A. Stocco, and M. Nobili, Nat. Mater. **14**, 908 (2015).
[39] V. N. Manoharan, Nat. Mater. **14**, 869 (2015).
[40] J. Koplik and C. Maldarelli, Phys. Rev. Fluids **2**, 024303 (2017).
[41] J. Toro-Mendoza, G. Rodriguez-Lopez, and O. Paredes-Altuve, Phys. Chem. Chem. Phys. **19**, 9092 (2017).
[42] G. Boniello, A. Stocco, C. Blanc, and M. Nobili, Phys. Chem. Chem. Phys. **19**, 22592 (2017).
[43] C. Snoeyink, S. Barman, and G. F. Christopher, Langmuir **31**, 891 (2015).
[44] M. Zanini and L. Isa, J. Phys. Condens. Matter **28**, 313002 (2016).
[45] E. J. Stancik, A. L. Hawkinson, J. Vermant, and G. G. Fuller, J. Rheol. **48**, 159 (2004).
[46] E. J. Stancik, G. T. Gavranovic, M. J. O. Widenbrant, A. T. Laschitsch, J. Vermant, and G. G. Fuller, Faraday Discuss. **123**, 145 (2003).
[47] P. L. Maffettone, M. Grosso, M. C. Friedenberg, and G. G. Fuller, Macromolecules **29**, 8473 (1996).
[48] T. Verwijlen, D. L. Leiske, P. Moldenaers, J. Vermant, and G. G. Fuller, J. Rheol. **56**, 1225 (2012).
[49] M. Dimitrijev-Dwyer and A. P. J. Middelberg, Soft Matter **7**, 7772 (2011).
[50] G. G. Fuller and J. Vermant, Annu. Rev. Chem. Biomol. Eng. **3**, 519 (2012)..